Bulletin of the Seismological Society of America, Vol. 108, No. 4, pp. 2237–2247, August 2018, doi: 10.1785/0120170276

Single-Station Standard Deviation Using Strong-Motion Data from Sichuan Region, China

by Ruizhi Wen, Peibin Xu, Hongwei Wang, and Yefei Ren

Abstract The standard deviation of ground-motion prediction equation under the ergodic assumption is commonly used for the site-specific probabilistic seismic hazard analysis. However, this assumption leads to overestimations of site-specific ground-motion variability. The single-station standard deviation (σ_{ss}) after removing the ergodic assumption on site response is therefore proposed for evaluating site-specific ground-motion variability. In this study, we evaluate σ_{ss} for the seismically active Sichuan region, China. Based on strong-motion data in this region, we first establish prediction equations for the sole purpose of computing means of ground-motion intensity measures (peak ground acceleration [PGA] and pseudospectral accelerations [PSAs]) for subsequent σ_{ss} analyses. Then, we apply 1463 recordings at a total of 47 stations to compute the σ_{ss} values. The standard deviations under the ergodic assumption range from 0.67 to 0.86 on the natural logarithmic scale, whereas σ_{ss} values range from 0.59 to 0.72, indicating the ~10%–20% reduction after removing the ergodic assumption on site response. The event-corrected single-station standard deviations (ϕ_{ss}) are reduced by about 15%–25% compared with the within-event standard deviation. The ϕ_{ss} values calculated in this study are generally higher than the usual values reported by previous studies. More heterogeneous propagation medium in this region, the boundary of the Sichuan basin and the eastern margin of the Tibet plateau, may cause larger ϕ_{ss} values than usual results. We infer that the use of aftershock recordings may be another reason for the large ϕ_{ss} values in that ruptures of mainshocks may amplify upper crust heterogeneity where seismic waves propagate during aftershocks. Therefore, the larger ϕ_{ss} values in this study could be a sort of warning against the usually assumed regional independency of ϕ_{ss} based on the usual values from previous studies.

Introduction

We are interested in site-specific ground-motion variability in probabilistic seismic hazard analysis (PSHA). Nearly all PSHAs are based on the ground-motion prediction equation (GMPE). The standard deviation (σ) of GMPE is commonly used to represent the variability of site-specific ground motions under the ergodic assumption that the uncertainty over time at a single point is treated as the spatial uncertainty of ground motions (Anderson and Brune, 1999). The standard deviation has significant influence on the results of PSHA, in particular at long return periods (Bommer and Abrahamson, 2006). In fact, it is inevitable that epistemic uncertainty (i.e., scientific uncertainty due to limited data and knowledge) is incorporated within aleatory variability in the development of a GMPE, which leads to the standard deviation overestimated with respect to the real situation (Anderson *et al.*, 2000). The key to decreasing standard deviation is to distinguish those components of ground-motion variability at a specific site that are repeatable sources, sites, and path effects, so that they can be removed from the total standard deviation. Al Atik *et al.* (2010) systematically identified these components of ground-motion variability at a specific site.

The single-station standard deviation (σ_{ss}), removing the ergodic assumption on site response, has recently been proposed as a more realistic estimation of ground-motion variability. Numerous previous studies evaluated σ_{ss} values using strong-motion recordings for different regions, for example, California (Atkinson, 2006), Japan (Rodriguez-Marek *et al.*, 2011, 2013), Taiwan (Lin *et al.*, 2011), New Zealand (Chen and Faccioli, 2013), Italy (Luzi *et al.*, 2014), Greece (Ktenidou *et al.*, 2017), Chile (Montalva *et al.*, 2017), and Iran (Zafarani and Soghrat, 2017). In all cases, these studies concluded that the σ_{ss} was significantly reduced with respect to the σ.

The new generation of the National Strong-Motion Observation Network System (NSMONS) has been operating in China since the end of 2007, and more than 1100 permanent free-field stations and 10 structural seismic response observation arrays now cover mainland China. NSMONS aims to improve the capability of earthquake monitor and the collection of strong-motion recordings in seismically active regions such as the Sichuan, Yunnan, and Xinjiang regions. There is a potentially high seismic hazard in Sichuan region after many destructive earthquakes (e.g., the 2008 M_s 8.0 Wenchuan, the 2013 M_s 7.0 Lushan, the 2014 M_s 6.3 Kangding, and the 2017 M_s 7.0 Jiuzhaigou earthquakes).

A range of GMPEs have been established for predicting ground motions in the Sichuan region. We note that prediction equations for this region were developed based mainly on recordings from the Wenchuan earthquake sequence, for example, Kang and Jin (2009), Yu and Li (2012), and Wang *et al.* (2013). Some equations for this region, including Lei *et al.* (2007), Kang and Jin (2009), and Wang *et al.* (2013), were developed solely for predicting ground motions on rock sites defined by the Code for Seismic Design of Buildings in China (GB 50011, 2010). Although the equation provided by Yu and Li (2012) considered V_{S30} values (time-weighted average shear-wave velocity over the upper 30 m) to characterize site effects, recordings from only 64 Wenchuan aftershocks were considered. These equations are not appropriate for the evaluation of the single-station standard deviation in the Sichuan region, due either to the lack of a site term or because a limited number of earthquakes were considered.

In this article, ground-motion recordings accumulated from the end of 2007 to the end of 2015 from earthquakes with M_s between 4.0 and 6.7 in the Sichuan region are used to evaluate the single-station standard deviation. To this end, we first establish prediction equations to calculate means of ground-motion intensity measures. Then, we systematically evaluate the single-station standard deviation.

Dataset

Between the end of 2007 to the end of 2015, more than 3900 three-component free-field strong-motion recordings were collected at 225 strong-motion stations of NSMONS from 688 earthquakes with M_s between 3.0 and 8.0 and focal depths less than, or equal to, 30 km in the Sichuan region. To establish prediction equations to compute means of ground motions in the Sichuan region for the single-station standard deviation evaluation, we constructed a dataset of strong-motion recordings according to the following criteria:

1. Recordings with Joyner–Boore distance $R_{JB} > 200$ km were excluded; recordings from earthquakes with $M_s \geq 7.0$ or < 4.0 were excluded; recordings from earthquakes with focal depths equal to zero were excluded; recordings obtained at stations with unavailable V_{S30} values were excluded.
2. We did not use more than one recording when multiple recordings from the same earthquake were recorded at the same site (e.g., within a differential array or by different sensors at the same site).
3. We used only recordings with three components, including one vertical and two horizontal components.
4. Poor-quality recordings were excluded following visual inspection, for example, recordings with multiple wave packets, severe drop tail, spikes, noise-dominated recordings, and unreliable recordings (i.e., those with extremely high or low amplitudes).
5. Earthquakes with fewer than four recordings were excluded after applying aforementioned selection criteria.

The final dataset used in this study consists of 1644 recordings obtained at 103 stations from 186 earthquakes, 125 of which are Wenchuan aftershocks, 39 of which are Lushan aftershocks, and 22 of which are other events in the Sichuan region. Earthquake epicenters and station locations are shown in Figure 1a,b. Figure 2a shows the M_s and R_{JB} distribution of recordings in this dataset. Recordings cover M_s in the 4.0–6.7 range, and R_{JB} ranges from 2 to 200 km. The relatively sparse data for $R_{JB} < 10$ km are all collected in events with $M_s < 5.5$. Because of unavailable finite-fault results, the simulation method proposed by Chiou and Youngs (2008) was used to estimate R_{JB} values based on limited source information, including hypocentral locations and focal mechanisms (if available in the Global Centroid Moment Tensor catalog) or the geometry of a seismogenic fault. This simulation method has been widely used to estimate R_{JB} values in the Next Generation Attenuation-West 2 (NGA-West2) flatfile.

The V_{S30} values for all 103 stations in this study are not directly measured from velocity profile for profiles depth $z_p \geq 30$ m; indeed, V_{S30} values for 89 out of the 103 stations were derived from the recommended values in the NGA-West2 site database (Seyhan *et al.*, 2014). In the case of 67 out of 89 stations, borehole velocity profile z_p was available, and the recommended V_{S30} values were inferred from the V_{SZ} values (the time-weighted average shear-wave velocity to z_p) according to the V_{S30}–V_{SZ} linear relationship proposed by Yu and Silva (in the Pacific Earthquake Engineering Research Center report of Ancheta *et al.*, 2013). For the remaining 22 out of the 89 stations, the recommended V_{S30} values were inferred from proxies that incorporate geomorphological- or terrain-based metrics, including geotechnical category, ground slope, and terrain-based categories. In the case of the remaining 14 stations that were not included in the NGA-West2 site database but that had borehole velocity profile $z_p < 30$ m, the V_{S30}–V_{SZ} extrapolation relationship proposed by Wang and Wang (2015) was used to infer V_{S30} values. This relationship provides the simple extrapolation of V_{S30} from V_{SZ1} and V_{SZ2} with $z1 < z2 \leq z_p$, and overcomes the inferred regional dependence of V_{S30}. In Figure 1b, stations with V_{S30} values derived from different approaches are distinguished using different colors. Figure 2b shows histograms of the V_{S30} values for the dataset used to develop the GMPE. These V_{S30} values are in the 227–649 m/s range. All data are for soil and soft rock sites (National Earthquake Hazards Reduction Program categories

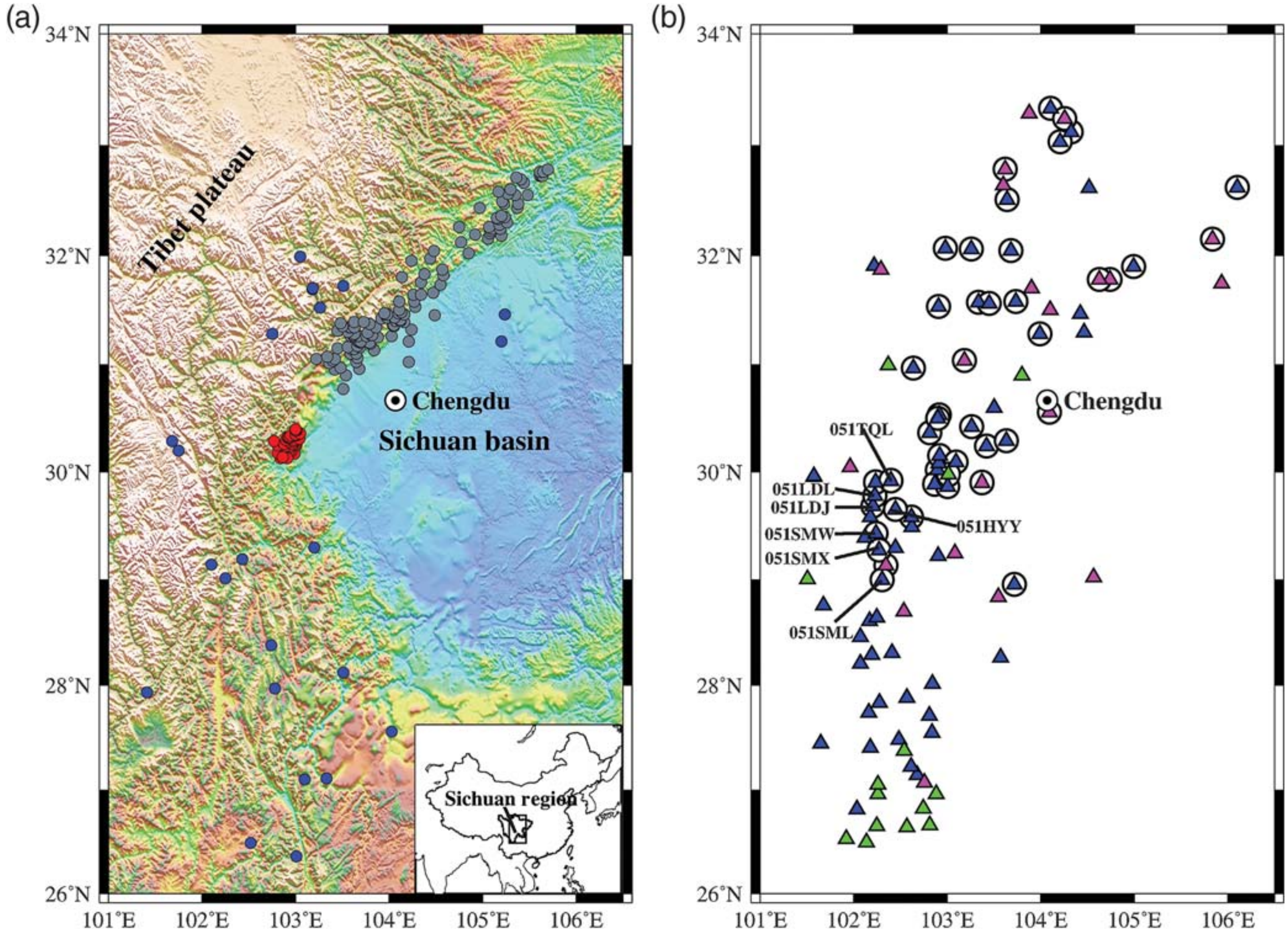

Figure 1. (a) Inset at bottom-right corner indicates the study area. Main figure: epicenters of earthquakes (gray, red, and blue circles) considered in this study. Gray, red, and blue circles are Wenchuan aftershocks, Lushan aftershocks and other events, respectively. (b) Locations of strong-motion stations (blue, magenta, and green triangles) considered in this study. Stations with different colors represent different sources of the V_{S30} values: blue, recommended values in Next Generation Attenuation-West 2 (NGA-West2) site database based on the V_{S30}–V_{SZ} relation of Yu and Silva; magenta, recommended values in NGA-West2 site database based on the geomorphologic- or terrain-based metrics, including geotechnical category, ground slope, terrain-based categories; green, inferred from the V_{S30}–V_{SZ} extrapolation relation of Wang and Wang (2015) based on the borehole velocity profile. Stations enclosed within circles were used to evaluate the single-station standard deviation.

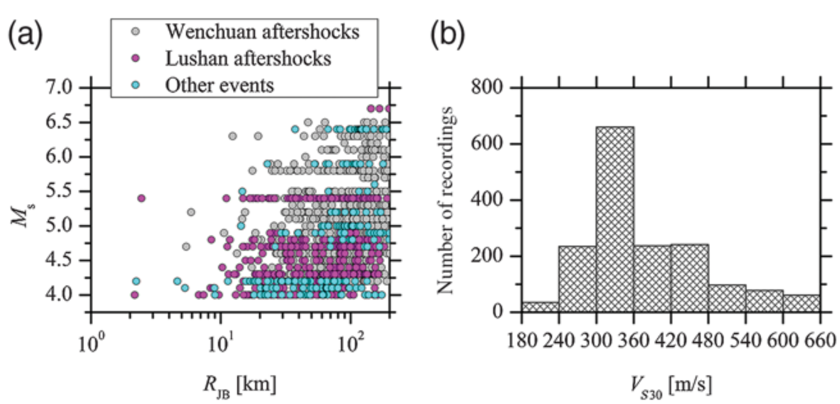

Figure 2. (a) Distribution of magnitude–distance for recordings in our dataset; (b) histogram of V_{S30} for recordings in our dataset.

C and D, with $360\ \mathrm{m/s} \le V_{S30} < 760\ \mathrm{m/s}$ and $180\ \mathrm{m/s} \le V_{S30} < 360\ \mathrm{m/s}$, respectively).

Recordings were processed using the low- and high-pass acausal Butterworth filters. The high-pass corner frequencies vary from 0.06 to 0.35 Hz, depending on the magnitude size. The low-pass corner frequency is uniformly set at 30 Hz. Visual inspections of Fourier amplitude spectra and integrated displacements for processed recordings were then also performed to ensure that appropriate corner frequencies had been selected. The minimum usable frequency was 0.075–0.44 Hz; that is, the high-pass corner frequency multiplied by a factor of 1.25 (Abrahamson and Silva, 1997). In this study, the usable frequency bandwidth extends from 25 to 0.5 Hz to ensure the same number of recordings at each frequency. The RotD50 is adopted as ground-motion intensity measure, which represents the median of the two horizontal-component time series combined into a single component by nonredundant azimuths (0°–180°; Boore, 2010).

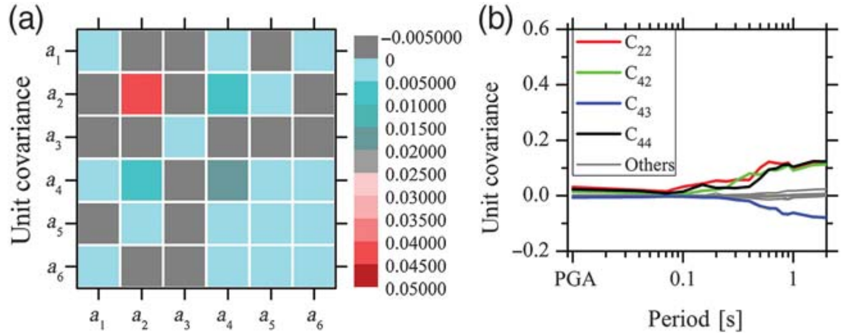

Figure 3. (a) The unit covariance matrix of any two coefficients for pseudospectral acceleration (PSA) at period of 0.1 s; (b) the unit covariance values of any two coefficients versus periods.

Prediction Equation

We developed a GMPE for the sole purpose of computing a mean of the ground-motion intensity measures, including peak ground acceleration (PGA) and 5% damped pseudospectral acceleration (PSA) for the Sichuan region to evaluate the single-station standard deviation. The GMPE is not expected to account for engineering predictions of ground motions and takes the source, path, and site effects using the main predictor variables into account, including M_s, R_{JB}, and V_{S30}. Ground-motion predictions are based on the following equation:

$$\ln Y = a_1 + a_2 M_s + a_3 \ln(R_{JB} + a_4 M_s) + a_5 R_{JB} + a_6 \ln(V_{S30}). \tag{1}$$

In this expression, in which $\ln Y$ denotes the natural logarithm of observed ground-motion intensity measures (i.e., PGA and PSAs), $a_1, a_2, \ldots, a_6$ are regression coefficients. The random-effects regression algorithm described by Abrahamson and Youngs (1992) was used in the regression analysis of equation (1); the regression coefficients, between-event and within-event standard deviations (τ and ϕ), and total standard deviation (σ) are listed in Table 1.

The unit covariance values of any two coefficients were calculated to determine if all those included in equation (1) are necessary and resolvable (Menke, 1989). The unit covariance matrix of any two coefficients for PSA at period of 0.1 s are plotted in Figure 3a; values in this case are all close to zero and within the range from −0.004 to 0.04, indicating that all coefficients do not show nonnegligible trade-offs for PSA at 0.1 s period. The unit covariance values of any two coefficients are plotted in Figure 3b; these data show that unit covariance values for $\alpha_2/\alpha_2(C_{22})$, $\alpha_2/\alpha_4(C_{24})$, $\alpha_4/\alpha_4(C_{44})$, and $\alpha_4/\alpha_3(C_{43})$ are remarkably large at periods over 0.1 s, whereas the remaining values are all close to zero. Indeed, results indicate that the magnitude–distance dependence term and the source term may exhibit trade-offs. These trade-offs might be explained by weak magnitude–distance dependence in our database due to the relatively small magnitude range (4.0–6.7) and few recordings at close distances (< 10 km), especially from earthquakes with $M_s > 5.5$. As magnitude–distance dependence (expressed as $\alpha_4 M$) is

Table 1
Regression Coefficients and the Standard Deviations for the Prediction Equation in This Study

Period (s)	a_1	a_2	a_3	a_4	a_5	a_6	τ	ϕ	σ	σ_{ss}	Bracketed σ_{ss}
PGA	0.5258	−1.7383	−1.0153	0.4079	−0.0006	−0.179	0.350	0.567	0.666	0.586	0.508
0.04	0.4795	−0.581	−1.0909	0.3091	−0.001	−0.2324	0.371	0.584	0.692	0.612	0.546
0.07	0.372	−0.0829	−0.8224	0.0004	−0.0037	−0.2906	0.387	0.628	0.737	0.619	0.541
0.1	0.424	−2.5172	−0.7561	0.1179	−0.0037	0.062	0.367	0.656	0.751	0.611	0.516
0.15	0.5756	−1.361	−1.0369	0.6515	0.0005	−0.1435	0.379	0.615	0.722	0.635	0.558
0.2	0.7036	−0.4274	−1.068	0.5227	0.0023	−0.4573	0.397	0.643	0.756	0.677	0.590
0.25	0.8015	−0.2861	−1.106	0.734	0.003	−0.5797	0.423	0.668	0.791	0.692	0.615
0.3	0.8744	−0.5572	−1.0537	0.8446	0.002	−0.6518	0.428	0.713	0.831	0.704	0.641
0.4	0.9853	−1.6343	−1.1456	1.2789	0.0023	−0.579	0.437	0.738	0.858	0.718	0.643
0.5	1.1077	−2.419	−1.3961	2.1221	0.0043	−0.4532	0.438	0.742	0.862	0.724	0.647
0.6	1.1826	−3.409	−1.459	2.2116	0.0049	−0.3747	0.438	0.718	0.841	0.712	0.644
0.7	1.2654	−3.8844	−1.5697	2.6472	0.0056	−0.3369	0.429	0.704	0.824	0.696	0.628
0.8	1.3528	−4.223	−1.7185	3.2653	0.0065	−0.2887	0.425	0.697	0.817	0.685	0.622
0.9	1.424	−4.6731	−1.8223	3.6521	0.0071	−0.2363	0.420	0.683	0.801	0.671	0.614
1	1.4813	−4.9102	−1.938	3.9169	0.008	−0.2009	0.417	0.666	0.786	0.659	0.609
1.5	1.613	−5.1808	−2.317	5.1049	0.0099	−0.1277	0.424	0.625	0.755	0.637	0.586
2	1.6769	−5.7163	−2.4086	5.379	0.0099	−0.12	0.411	0.677	0.792	0.637	0.577

PGA, peak ground acceleration.

commonly considered in GMPEs, we still included it in our equation.

We next evaluated the residuals between observations and predictions from equation (1). Residual R_{es} of the observation at station s of the earthquake e is calculated as follows:

$$R_{es} = \ln Y_{es} - \mu_{es}(M_s, R_{JB}, V_{S30}), \quad (2)$$

in which μ_{es} denotes the prediction from equation (1) and $\ln Y_{es}$ is the natural logarithm of the observation. Generally, R_{es} can be decomposed into the between-event residual (δB_e) and the within-event residual (δW_{es}), which are zero-mean, independent, normally distributed random variables with standard deviations τ and ϕ, respectively. The δB_e is the average deviation of the observed ground motion from an earthquake e with respect to the mean of the predicted ground motion. The δW_{es} is the difference between an individual observation at the station s and the specific-earthquake mean prediction.

The between-event residuals (δB_e) against M_s for PGA and PSAs at 0.2, 1.0, and 2.0 s periods are plotted in Figure 4a. We note that δB_e values do not show any obvious trends with respect to M_s, and the magnitude-binned means slightly fluctuate around zero. The magnitude-binned means of δB_e values at all considered periods from 0.04 to 2.0 s are all independent of M_s and close to zero, and indicate that there are no magnitude-scaling errors.

The δW_{es} values at station s can be used to further estimate its site term ($\delta S2S_s$), expressed as

$$\delta S2S_s = \frac{1}{NE_s} \sum_{e=1}^{NE_s} \delta W_{es}, \quad (3)$$

in which NE_s is the number of earthquakes recorded by station s. The site term $\delta S2S_s$ reflects the deviation of the actual amplification at station s from the predicted amplification characterized by simple site parameters (e.g., V_{S30}). Positive $\delta S2S_s$ value means that actual amplification is underestimated, negative $\delta S2S_s$ value indicates that actual amplification is overestimated, and $\delta S2S_s$ equal to zero indicates that the site effects are exactly as predicted. The data in Figure 4b show $\delta S2S_s$ values against V_{S30} for PGA and PSAs at 0.2, 1.0, and 2.0 s periods. The $\delta S2S_s$ values do not show any trend with V_{S30}, and the V_{S30}-binned means are approximately zero. V_{S30}-binned means across all periods considered show the zero mean and a flat trend with V_{S30}, indicating that there are no site-scaling errors.

Figure 4c shows event- and site-corrected residuals ($\delta W_{o,es}$) versus R_{JB} for PGA and PSAs at 0.2, 1.0, and

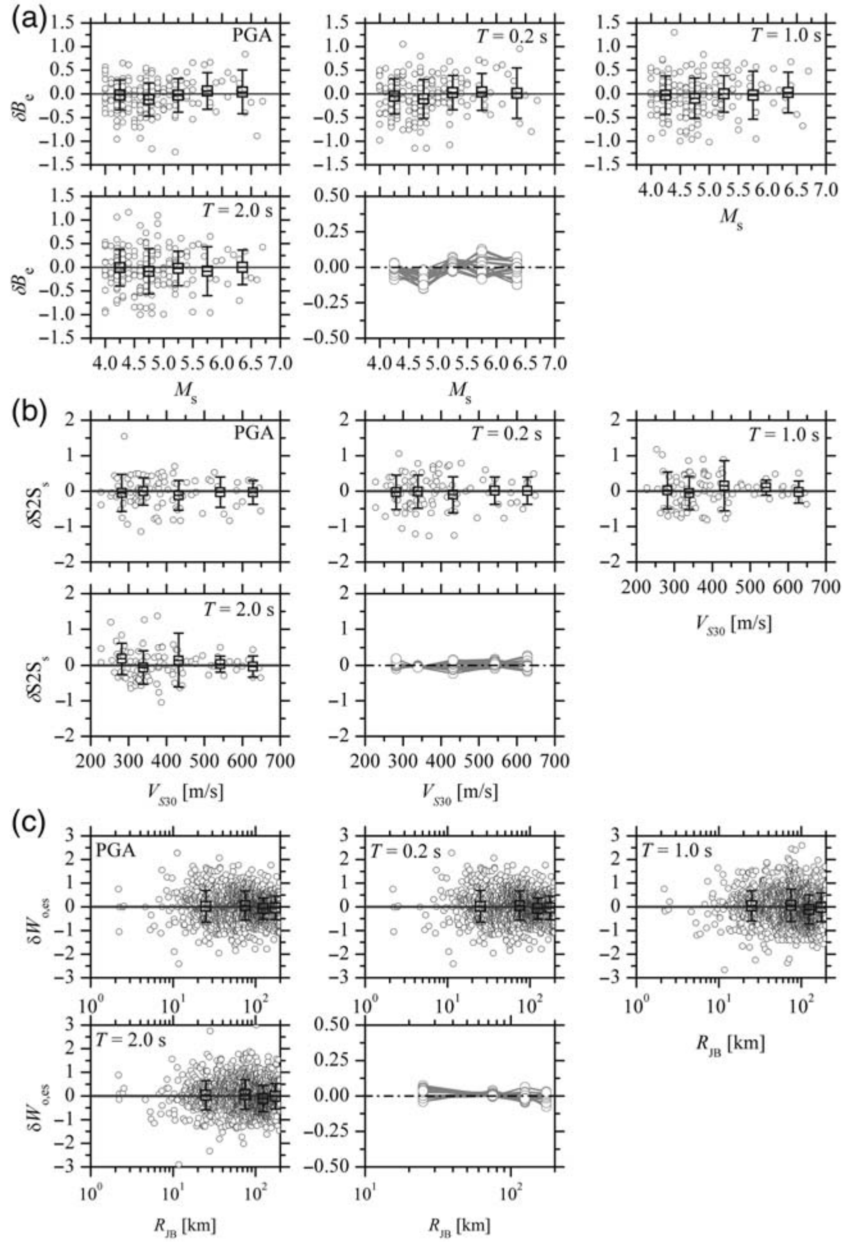

Figure 4. (a) Between-event residuals δB_e for the peak ground acceleration (PGA) and PSAs at periods of $T = 0.2$, 1.0, and 2.0 s against surface magnitude M_s. The magnitude-binned means and standard deviations in five bins were plotted. The magnitude-binned means at all periods considered were also shown; (b) the site term $\delta S2S_s$ for the PGA and PSAs at 0.2, 1.0, and 2.0 s periods against V_{S30}. The V_{S30}-binned means and standard deviations in five bins were plotted. The V_{S30}-binned means at all periods considered were also shown. (c) The event- and site-corrected residuals $\delta W_{o,es}$ for the PGA and PSAs at 0.2, 1.0, and 2.0 s periods against Joyner–Boore distance R_{JB}. The distance-binned means and standard deviations in four bins were plotted. The distance-binned means at all periods considered were also shown.

2.0 s periods. The $\delta W_{o,es}$ can be obtained by subtracting the $\delta S2S_s$ from δW_{es}. The $\delta W_{o,es}$ values do not show any trend with R_{JB}, and the distance-binned means with a width of 50 km are close zero. The distance-binned means of $\delta W_{o,es}$ at all considered periods show a flat trend around zero, indicating that there are no distance-scaling errors.

Figure 5 shows the within-event standard deviation ϕ and the between-event standard deviation τ in our equation. In this case, ϕ-values, which range from ~0.57 to ~0.74, increase as the period approaches 0.4 s, before they peak and then decrease again. In contrast, τ-values vary within a range between 0.35 and 0.44, and exhibit principle positive increasing trend as the period increases. We also compared these values with the ϕ- and τ-values from some other prediction equations, for example, the ASK14 model proposed by Abrahamson *et al.* (2014), the BSSA14 model proposed by Boore *et al.* (2014), and the pan-European model proposed by Bindi *et al.* (2014). The pan-European model was established using strong-motion recordings in Europe and the Middle East; the ASK14 and BSSA14 models were established in the NGA-West2 project for ground-motion prediction of global shallow crustal earthquakes. The ϕ- and τ-values are dependent on magnitude in the ASK14 and BSSA14 models. The ranges of ϕ- and τ-values for these models are also plotted in Figure 5. The ϕ- and τ-values for the effects of linear site response were considered in the ASK14 model. The ϕ-values in this study fall within the ranges of the ASK14 and BSSA14 models, except for slightly larger values in the periods from 0.3 to 1.0 s (0.67–0.74). We obtain slightly smaller τ-values in this study than those in other models at ≤ 0.1 s periods, but share approximately consistent results at periods between 0.15 s and 2.0 s.

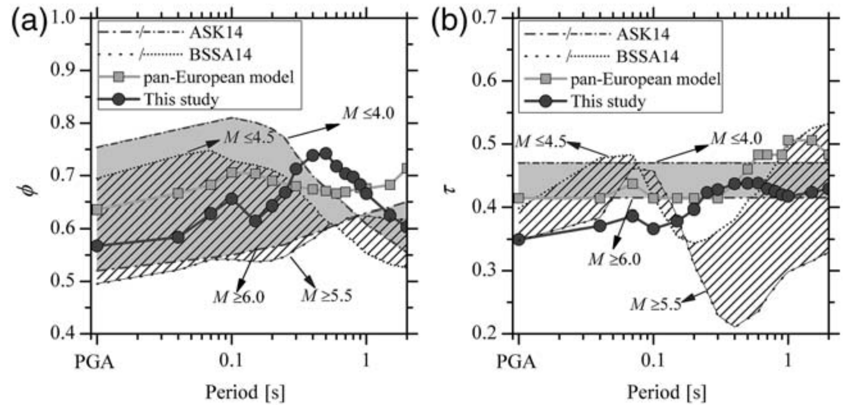

Figure 5. (a) Within-event standard deviations ϕ and (b) between-event standard deviations τ in this study. The ϕ- and τ-values in prediction models, including the BSSA14 model by Boore *et al.* (2014), the ASK14 model by Abrahamson *et al.* (2014), and the pan-European model by Bindi *et al.* (2014) are also shown. Shaded areas indicate the varied ranges of ϕ- and τ-values, dependent on the magnitude in ASK14 and BSSA14 models.

Single-Station Standard Deviation

To evaluate single-station standard deviation in the Sichuan region, recordings from stations that recorded at least 10 events in the aforementioned database are considered because too few recordings at a station make for unreliable site terms $\delta S2S_s$. Thus, to compute the single-station standard deviation (σ_{ss}), we consider 1463 recordings from a total of 47 stations (enclosed within the circle in Fig. 1b and listed in Table 2), 21 of which are class C sites and 26 of which are class D sites.

Table 2
Information of the Selected Stations for Single-Station Standard Deviation Analysis

Station Code	Number of Recordings	V_{S30} (m/s)	Station Code	Number of Recordings	V_{S30} (m/s)
051BXD*	30	585	051LXS†	54	341
051BXY†	27	305	051LXT†	89	351
051BXZ†	23	394	051MCL†	10	453
051CDZ*	14	297	051MXD†	91	268
051GYS*	12	388	051MXN†	80	383
051GYZ†	12	395	051PJD†	33	390
051HSD†	33	345	051PJW†	24	338
051HSL†	34	288	051QLY†	27	535
051HYQ†	12	286	051SFB†	23	379
051HYT*	19	437	051SMC*	10	319
051HYY†	19	475	051SML†	23	326
051JYC†	74	466	051SMW†	16	305
051JYD*	42	478	051SMX†	24	323
051JYH*	52	320	051SPA†	42	333
051JZB†	13	328	051SPC*	15	374
051JZG†	33	297	051TQL†	27	526
051JZW†	40	430	051WCW*	31	356
051JZY*	28	326	051XJB‡	16	318
051LDJ†	30	288	051XJD‡	12	336
051LDL†	32	327	051YAD‡	33	228
051LDS†	19	349	051YAL†	27	535
051LSF†	11	517	051YAM†	27	600
051LSJ†	26	587	051YAS†	19	437
051LXM†	75	306			

*Recommended values in Next Generation Attenuation-West 2 (NGA-West2) site database based on the geomorphologic- or terrain-based metrics, including geotechnical category, ground slope, and terrain-based categories.

†Recommended values in NGA-West2 site database based on the V_{S30}–V_{SZ} relation of Yu and Silva.

‡Inferred from the V_{S30}–V_{SZ} extrapolation relation of Wang and Wang (2015) based on the borehole velocity profile.

First, the $\delta S2S_s$ values for all stations analyzed were calculated according to equation (3); in this case, Figure 6a shows $\delta S2S_s$ values for three typical stations, 051BXD, 051LSF, and 051MXD. The 051BXD station shows a flat trend around zero, indicating a good representation of the site effect using only the V_{S30} value in the prediction equation. Pronounced deviations to zero at stations 051LSF and 051MXD indicate that the actual site effects are either overestimated or underestimated by the prediction equation. The V_{S30} is used to represent only the site effects in the predictions. In fact, some other site factors, including local topography, geological structures more than 30 m below the surface, and soil layer characteristics also exert important impacts on ground motion. The obvious peak at ~0.15 s at station 051LSF may be the result of topographic effects (Wen and Ren, 2014). The station 051MXD shows considerably high $\delta S2S_s$ values (0.75–1.25) during periods of 0.3–2.0 s, and low $\delta S2S_s$ values (~ -0.5) before 0.1 s. The borehole velocity profile up to 21 m (Fig. 6b) reveals low-velocity soft soil with $V_S = 150$–400 m/s at this station, and we infer that the underestimations at intermediate-to-long periods as well as the short-period overestimations may have been caused by a deep soft soil layer, 30 m or more.

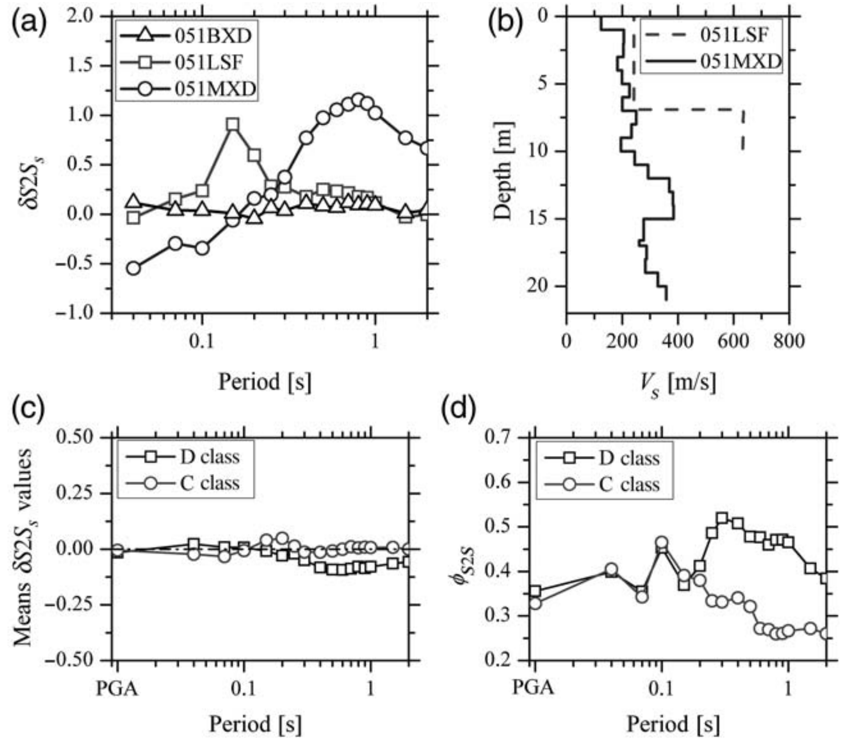

Figure 6. (a) The $\delta S2S_s$ values at 0.04–2.0 s periods for three typical stations, 051BXD, 051LSF, and 051MXD; (b) the shear-wave velocity borehole profiles for stations 051LSF and 051MXD; (c) means of $\delta S2S_s$ values over class C and D sites, respectively; (d) standard deviations of $\delta S2S_s$ values (ϕ_{S2S}) for class C and D sites, respectively.

As mentioned above, stations analyzed are classified as class C and D sites. The means of $\delta S2S_s$ values for stations within each class are plotted in Figure 6c. The means of $\delta S2S_s$ values for class C sites are always in close proximity to zero, indicating the good predictions of site term at class C sites. However, the class D sites just show the approximately zero means at ≤ 0.3 s periods. The negative means for class D sites observed at periods between 0.3 and 2.0 s illustrate a general overestimation of the site term for soil sites. The standard deviation of $\delta S2S_s$, denoted by ϕ_{S2S}, quantifies the site-to-site variability for the class C and D sites, respectively. The class C and D sites share approximately consistent ϕ_{S2S} values before 0.2 s, as shown in Figure 6d. However, we observe that the ϕ_{S2S} values for class D sites are significantly higher than those for class C sites after 0.2 s. This shows that softer sites cause larger variability of site effects.

The single-station standard deviation σ_{ss} can be expressed as follows:

$$\sigma_{ss} = \sqrt{\phi_{ss}^2 + \tau^2} \tag{4}$$

and

$$\phi_{ss} = \sqrt{\frac{\sum_{s=1}^{NS} \sum_{e=1}^{NE_s} \delta W_{o,es}^2}{(\sum_{s=1}^{NS} NE_s) - 1}}. \tag{5}$$

The ϕ_{ss} stands for the event-corrected single-station standard deviation over all stations analyzed, and $NS = 47$ represents the total number of stations analyzed. Similar to equation (5), the event-corrected single-station standard deviation for station $s(\phi_{ss,s})$, which reflects ground-motion variability at this station, can be given as follows:

$$\phi_{ss,s} = \sqrt{\frac{\sum_{e=1}^{NE_s} \delta W_{o,es}^2}{NE_s - 1}}. \tag{6}$$

The $\phi_{ss,s}$ values ($s = 1 - NS$) calculated for PGA and PSAs over the periods between 0.04 and 2.0 s are shown in Figure 7a. The $\phi_{ss,s}$ values show significant differences among stations, which could be interpreted as the result of multiple sources and various paths for a specific station. Thus, to clearly show the differences between the mean and median over NS stations, the ratios between both values on the natural logarithmic scale are plotted in Figure 7b. The medians are smaller than the means for PGA and PSAs at periods between 0.04 and 0.2 s, at 0.4 s, and between 0.8 and 2.0 s, indicative of right-skewed distribution, whereas larger medians than means for PSAs at periods between 0.25 and 0.3 s and between 0.5 and 0.7 s indicate a left-skewed distribution.

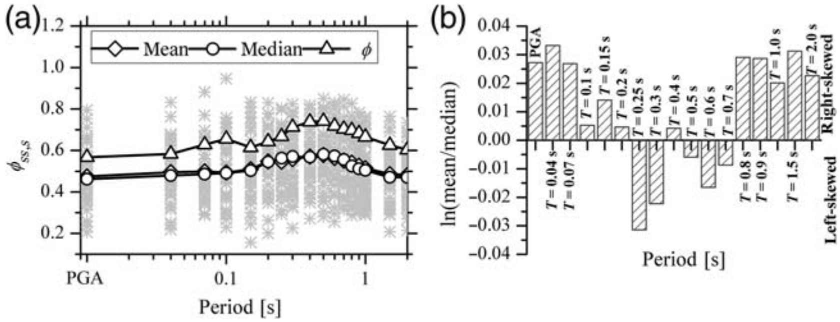

Figure 7. (a) The event-corrected single-station standard deviation for each station ($\phi_{ss,s}$) considered in this study. The medians and means of $\phi_{ss,s}$ values over all stations and the ϕ-values in Table 1 were also plotted for PGA and PSAs at periods of $T = 0.04$–2.0 s, respectively. (b) Comparisons between the means and the medians of $\phi_{ss,s}$ values.

The skewed distributions dependent on the periods in our study are inconsistent with the uniformly right-skewed distributions reported by Rodriguez-Marek *et al.* (2011).

Figure 8 shows the ϕ_{ss} values computed according to equation (5). The ϕ_{ss} values are in the 0.47–0.58 range for PGA and PSAs at periods between 0.04 and 2.0 s. A striking result is observed: the ϕ_{ss} values in the function of periods show obvious bump at 0.2–1.0 s periods and the larger ϕ_{ss} values (> 0.5) appear. The ϕ-values listed in Table 1 also show a similar bump at these periods. The reason for this bump is not explicit to date and needs to be further investigated. Compared with ϕ-values, the ϕ_{ss} values are reduced by ~15%–25%. The ϕ_{ss} values calculated for different regions in the previous studies are also plotted in Figure 8, including California, Switzerland, Taiwan, Turkey, and Japan (Rodriguez-Marek *et al.*, 2011, 2013), the Canterbury region in New Zealand (Chen and Faccioli, 2013), Italy (Luzi *et al.*, 2014), Greece (Ktenidou *et al.*, 2017), Chile (Montalva *et al.*, 2017), and Iran (Zafarani and Soghrat, 2017). The usual ϕ_{ss} values, ranging from ~0.4 to ~0.5, are generally obtained in the other regions (represented by the gray bars in Fig. 8), except for smaller ϕ_{ss} values in Greece and Chile and larger ϕ_{ss} values in Iran and California. According to these usual ϕ_{ss} values, ϕ_{ss} is usually assumed to be independent of region. The ϕ_{ss} values for PGA and PSAs for short periods (≤ 0.1 s) in our study are close to the usual results. However, these values at long periods (> 0.1 s) are significantly larger than the usual values, but close to those reported for California and Iran. Meanwhile, the downward trend of the usual ϕ_{ss} values over 0.3 s does not appear in our study region or Iran. The lower ϕ_{ss} values for Greece and Chile might be somewhat peculiar. The low values (~0.30) for Greece might be the result of a test site analyzed where stations are situated close to one another in a narrow area, whereas large earthquakes in a subduction setting might have caused these low values in Chile. In spite of these results in Greece and Chile, the larger ϕ_{ss} values in our study region, as well as California and Iran, are a sort of warning against the assumption that ϕ_{ss} is regionally independent.

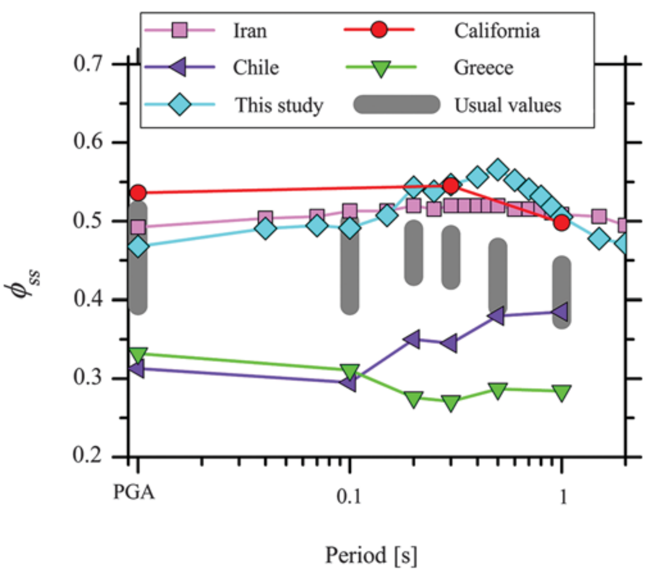

Figure 8. The event-corrected single-station standard deviations (ϕ_{ss}) for the Sichuan region in this study. The usual values represented by the gray bars (including Switzerland, Taiwan, Turkey, and Japan: Rodriguez-Marek *et al.*, 2011, 2013; Italy: Luzi *et al.*, 2014; Canterbury region in New Zealand: Chen and Faccioli, 2013), small ϕ_{ss} values for Greece (Ktenidou *et al.*, 2017) and Chile (Montalva *et al.*, 2017), and large ϕ_{ss} values for California (Rodriguez-Marek *et al.*, 2013) and Iran (Zafarani and Soghrat, 2017) were compared with our results.

The ϕ_{ss} reflects the ground-motion variability due to heterogeneity of the propagation medium for the entire region, according to equation (5). The potential discrepancies in propagation medium heterogeneity in different regions may be a challenge to the usual regional independency of ϕ_{ss}. Our study region is located on the boundary of the Sichuan basin and the eastern margin of the Tibet plateau, across which substantial differences in crustal structure have been reported (Wang *et al.*, 2007; Li *et al.*, 2012). Large values of ϕ_{ss} might be expected given the high heterogeneity of crustal medium in our study region. Furthermore, recordings used in this study are collected mainly from the Wenchuan and Lushan aftershocks, which are distributed along ruptured faults after the mainshocks, and which may amplify the upper crust heterogeneity. Similarly, the large ϕ_{ss} values for Iran reported by Zafarani and Soghrat (2017) are derived from the bulk of recordings from earthquakes that could be classified as aftershocks. The use of aftershock recordings may be an additional reason for the large ϕ_{ss} values in that ruptures in the mainshocks may amplify the crustal medium variability where seismic waves propagate during aftershocks.

It is well known that seismic waves mainly propagate through the upper crust over local distances, but predominantly propagate through the Moho over regional distances.

To further verify the large ϕ_{ss} values obtained in this study, the ϕ_{ss} values based on recordings in four R_{JB} bins (< 50, 50–100, 100–150, and > 150 km) are plotted in Figure 9. The ϕ_{ss} values for R_{JB} < 50 km range between ~0.55 and 0.65, significantly high for PGA and PSAs. We note that the ϕ_{ss} values for the remaining three distance bins do not show remarkable changes and range from 0.40 to 0.55. The ϕ_{ss} values for $R_{\mathrm{JB}} = 50$–100 km are approximately equal to the results in our study with an average of 0.53. For the R_{JB} bins of 100–150 and > 150 km, the ϕ_{ss} values are very close to the usual results (0.4–0.5) reported in other studies (Rodriguez-Marek *et al.*, 2011, 2013; Chen and Faccioli, 2013; Luzi *et al.*, 2014). Following the distance-dependent ϕ_{ss} values, the larger variability at local distances of R_{JB} < 50 km contributes to the higher ϕ_{ss} values in this study. We also note that the number of recordings in the three small R_{JB} bins are approximately identical (403, 504, and 396), except for a few recordings for R_{JB} > 150 km (160). The higher ϕ_{ss} values for R_{JB} < 50 km may be due to higher propagation medium heterogeneity, rather than too few recordings in the bin.

We further attempt to represent the effects of path variability on the ϕ_{ss}. For this purpose, the bracketed ϕ_{ss} values are calculated using recordings obtained at stations within a 10° bracket of event-to-station azimuths. The bracketed ϕ_{ss} values limit the recordings at a station as much as possible to narrow event-to-station azimuth coverage to exclude sparse ray paths. The following criteria are applied to select recordings for the bracketed ϕ_{ss} computations: (1) a station could be considered only if the number of recordings within a 10° bracket of event-to-station azimuth was not fewer than 10, and (2) if one station has more than one available 10° bracketed coverage where the number of recordings was at least 10, recordings within the bracketed coverage with the maximum recording number are used. We apply 327 recordings at 21 of the 47 stations to compute the bracketed ϕ_{ss} values, as shown in Figure 10a. The bracketed ϕ_{ss} values are in the 0.40–0.51 range and demonstrate an 8%–18% reduction compared to ϕ_{ss} values. Compared with the 7%–13% reduction estimated from a 10° bracketed database in Japan (Rodriguez-Marek *et al.*, 2011), the larger reduction may imply remarkable path variability in our study region.

Meanwhile, clusters of the Lushan aftershocks, recorded by several stations in our study, provide a good chance to analyze event-corrected single-path single-station standard deviation ϕ_{ss-sp}. Recordings obtained at seven stations (051HYY, 051LDJ, 051LDL, 051TQL, 051SML, 051SMW, and 051SMX, marked in Fig. 1b) in the Lushan aftershocks are used to compute the ϕ_{ss-sp} values, as shown in Figure 10a. The Lushan events are located northeast of these stations, with the event-to-station azimuth coverage ranging from 20.5°–29.8° to 50.2°–60.2°, and the distance coverage ranging from 49.6–77.1 to 141.9–168.3 km. The propagation paths from these stations to the Lushan events could be approximately considered a single path. More significantly, the ϕ_{ss-sp} values ranging from 0.32 to 0.50 indicate a 11%–35% reduction with respect to the ϕ_{ss} values. The ϕ_{ss-sp} values are similar to the bracketed ϕ_{ss} values at periods over 0.2 s, and much lower than the bracketed ϕ_{ss} values at periods below 0.2 s. This implies propagation path heterogeneity is a large factor in the variability of high-frequency ground motions.

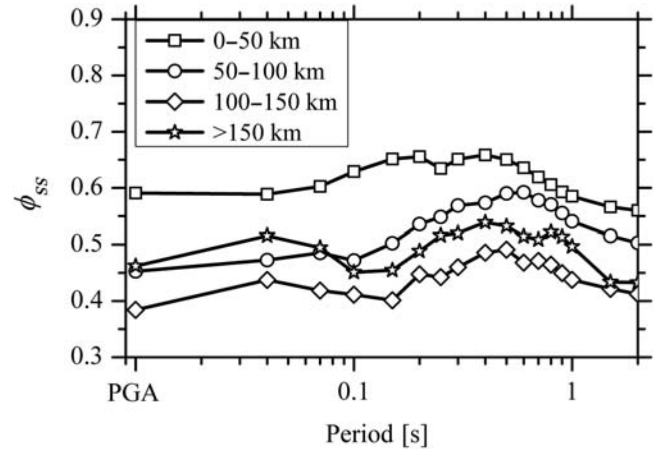

Figure 9. The event-corrected single-station standard deviations (ϕ_{ss}) from recordings within four distance bins (R_{JB} < 50, 50–100, 100–150, and > 150 km), respectively.

The closeness index (CI) proposed by Lin *et al.* (2011) has been calculated for the total and the bracketed datasets, respectively, to explain the path variability in the ϕ_{ss}. The CI value ranges from 0 for collocated earthquakes to 2 for earthquakes located in opposite epicentral directions from the site. The proportions of recordings within different CI bins, accounting for the total number of recordings, are given in Figure 10b. Relatively more recordings show smaller CI values (< 1.0) in the bracket dataset, while larger CI

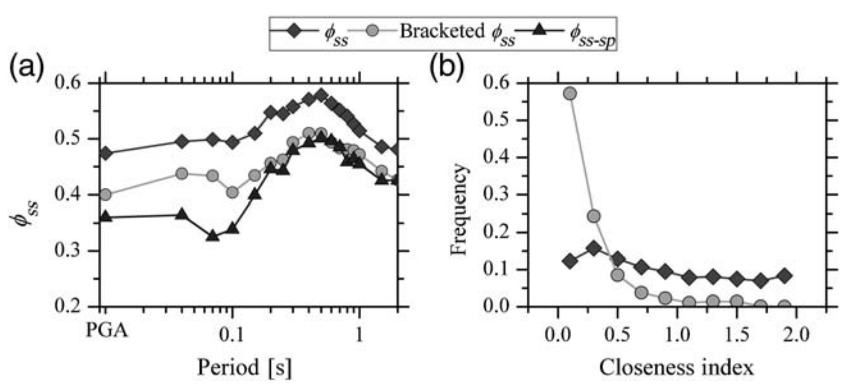

Figure 10. (a) The ϕ_{ss} values, the 10° bracketed ϕ_{ss} values, and the ϕ_{ss-sp} values; (b) proportions of recordings within different bins of closeness index accounting for the total number of recordings in the total and bracket databases, respectively.

values (> 1.0) are more prevalent in the total dataset. This further indicates that path variability is a significant factor in the computed ϕ_{ss} values.

According to the ϕ_{ss} values, σ_{ss} values are calculated and listed in Table 1. The σ_{ss} values decrease to ~0.59–0.72, and when compared with the σ-values with the ergodic assumption (~0.67–0.86) listed in Table 1, indicate a reduction of ~10%–20%.

Conclusions

Compared with the generally overestimated standard deviation of the GMPE, the single-station standard deviation (σ_{ss}) is reduced after removing the ergodic assumption on site response, and reasonably represents the site-specific ground-motion variability in the PSHA. In this study, the single-station standard deviations for the seismically active Sichuan region are evaluated using strong-motion recordings from earthquakes in this region from the end of 2007 until to the end of 2015. First, prediction equation providing a mean of the ground motion in this region is established for the sole purpose of σ_{ss} analysis. The residual analyses confirm that there are no magnitude-scaling, site-scaling, and distance-scaling errors. The standard deviations under the ergodic assumption ranged from 0.67 to 0.86 on the natural logarithmic scale (Table 1), whereas the resultant σ_{ss} values are in the 0.59–0.72 range and indicate a 10%–20% reduction after removing the ergodic assumption on site response.

The ϕ_{ss} values, ranging from 0.47 to 0.58, are generally higher than the usual values (~0.4–0.5), especially at periods between 0.2 and 1.0 s. These larger ϕ_{ss} values are observed not only in our study, but also in data from California (Rodriguez-Marek *et al.*, 2013) and Iran (Zafarani and Soghrat, 2017). The ϕ_{ss} reflects the ground-motion variability due to the propagation medium heterogeneity for the entire region under investigation. The Sichuan region analyzed in this study is located on the boundary of the stable Sichuan basin and the active eastern margin of the Tibet plateau. High crust heterogeneity may have caused the large ϕ_{ss} values obtained in this study. Furthermore, recordings considered in this study are mainly collected from the Wenchuan and Lushan aftershocks, distributed along the ruptured fault of the mainshock. We infer that the use of aftershock recordings may be an additional reason for the large ϕ_{ss} values, in that ruptures of the mainshocks may amplify the upper crust heterogeneity where seismic waves propagate during aftershocks. More heterogeneous propagation medium in this region causes larger ϕ_{ss} values than the usual results. This is also verified by distance-dependent ϕ_{ss} values that larger ϕ_{ss} values are observed for local distances ($R_{JB} < 50$ km). Therefore, the larger ϕ_{ss} values in this study could be a sort of warning against the usual assumption that ϕ_{ss} is regionally independent, an assumption based on the usual values from some previous studies.

Data and Resources

Strong-motion recordings used in this article were obtained from the China Strong-Motion Networks Center at http://www.csmnc.net/ (last accessed December 2015). Please note that this website is currently under maintenance and official notice by the Institute of Engineering Mechanics, CEA can be obtained at http://www.iem.ac.cn/detail.html?id=1102 (last accessed June 2018). During the period of maintenance, please contact csmnc@iem.ac.cn for data application. The earthquakes magnitudes were obtained from China Earthquake Network Center (http://news.ceic.ac.cn/, last accessed December 2015). The Global Centroid Moment Tensor catalog is available for download at www.globalcmt.org (last accessed September 2017). The V_{S30} values were obtained from the Next Generation Attenuation-West 2 (NGA-West2) site database of the Pacific Earthquake Engineering Research Center at http://peer.berkeley.edu/nga/ (last accessed March 2014). Figure 1a,b was produced using Generic Mapping Tools (Wessel and Smith, 1991).

Acknowledgments

The authors are very grateful to Adrian Rodriguez-Marek, Dino Bindi, Olga Ktenidou, and anonymous reviewers for their valuable comments and suggestions that improved this article. This work was supported by the Science Foundation of Institute of Engineering Mechanics, China Earthquake Administration (CEA) under Grant Number 2016A04, National Natural Science Fund Numbers 51778589 and U1534202, and the Natural Science Fund of Heilongjiang Province Number E2017065.

References

Abrahamson, N. A., and W. J. Silva (1997). Empirical response spectral attenuation relations for shallow crustal earthquakes, *Seismol. Res. Lett.* **68,** 94–127.

Abrahamson, N. A., and R. R. Youngs (1992). A stable algorithm for regression analyses using the random effects model, *Bull. Seismol. Soc. Am.* **82,** 505–510.

Abrahamson, N. A., W. J. Silva, and R. Kamai (2014). Summary of the ASK14 ground-motion relation for active crustal regions, *Earthq. Spectra* **30,** 1024–1056.

Al Atik, L., N. A. Abrahamson, J. J. Bommer, F. Scherbaum, F. Cotton, and N. Kuehn (2010). The variability of ground-motion prediction models and its components, *Seismol. Res. Lett.* **81,** 794–801.

Ancheta, T. D., R. B. Darragh, J. P. Stewart, E. Seyhan, W. J. Silva, B. S. J. Chiou, D. E. Wooddell, R. W. Graves, A. R. Kootke, D. M. Boore, *et al.* (2013). NGA-West2 database, *PEER Report 2013/03*, Pacific Earthquake Engineering Research Center, Berkeley, California.

Anderson, J., J. Brune, R. Anooshehpoor, and S. Ni (2000). New ground motion data and concepts in seismic hazard analysis, *Curr. Sci.* **79,** 1278–1290.

Anderson, J. G., and J. N. Brune (1999). Probabilistic seismic hazard assessment without the ergodic assumption, *Seismol. Res. Lett.* **70,** 19–28.

Atkinson, G. M. (2006). Single-station sigma, *Bull. Seismol. Soc. Am.* **96,** 446–455, doi: 10.1785/0120050137.

Bindi, D., M. Massa, L. Luzi, G. Ameri, F. Pacor, R. Puglia, and P. Augliera (2014). Pan-European ground-motion prediction equations for the average horizontal component of PGA, PGV, and 5%-damped PSA at spectral periods up to 3.0 s using the RESORCE dataset, *Bull Earthq. Eng.* **12,** 391–430.

Bommer, J. J., and N. A. Abrahamson (2006). Why do modern probabilistic seismic-hazard analyses often lead to increased hazard estimates? *Bull. Seismol. Soc. Am.* **96,** 1967–1977.

Boore, D. M. (2010). Orientation-independent, nongeometric-mean measures of seismic intensity from horizontal components of motion, *Bull. Seismol. Soc. Am.* **100,** 1830–1835.

Boore, D. M., J. P. Stewart, E. Seyhan, and G. M. Atkinson (2014). NGA-West 2 equations for predicting PGA, PGV and 5% damped PSA for shallow crustal earthquakes, *Earthq. Spectra* **30,** 1057–1086.

Chen, L. W., and E. Faccioli (2013). Single-station standard deviation analysis of 2010-2012 strong-motion data from the Canterbury region, New Zealand, *Bull. Earthq. Eng.* **11,** 1617–1632.

Chiou, B. S. J., and R. R. Youngs (2008). NGA model for average horizontal component of peak ground motion and response spectral, *PEER Report 2008/09*, Pacific Earthquake Engineering Research Center, Berkeley, California.

GB 50011 (2010). *Code for Seismic Design of Buildings*, China Architecture Industry Press, Beijing, China (in Chinese).

Kang, L. C., and X. Jin (2009). Ground motion attenuation relation for small to moderate earthquake in Sichuan region, *Acta Seismol. Sinica* **31,** 403–410 (in Chinese).

Ktenidou, O.-J., Z. Roumelioti, N. Abrahamson, F. Cotton, K. Pitilakis, and F. Hollender (2017). Understanding single-station ground motion variability and uncertainty (sigma): Lessons learnt from EUROSEISTEST. *Bull. Earthq. Eng.* 1–26, doi: 10.1007/s10518-017-0098-6.

Lei, J. C., M. T. Gao, and Y. X. Yu (2007). Seismic motion attenuation relations in Sichuan and adjacent areas, *Acta Seismol. Sinica* **29,** 500–511 (in Chinese).

Li, Z. W., S. D. Ni, T. Y. Hao, Y. Xu, and S. Roecker (2012). Uppermost mantle structure of the eastern margin of the Tibetan plateau from interstation *Pn* travel time difference tomography, *Earth Planet. Sci. Lett.* **335/336,** 195–205.

Lin, P. S., N. Chiou, M. Abrabamson, M. Walling, C. T. Lee, and C. T. Cheng (2011). Repeatable source, site and path effects on the standard deviation for empirical ground-motion prediction models, *Bull. Seismol. Soc. Am.* **101,** 2281–2295.

Luzi, L., D. Bindi, R. Puglia, F. Pacor, and A. Oth (2014). Single-station sigma for Italian strong-motion stations, *Bull. Seismol. Soc. Am.* **104,** 467–483.

Menke, W. (1989). *Geophysical Data analysis: Discrete Inverse Theory*, in IntGeophys Series, R. Dmowska and J. R. Holton (Editors), Vol. 45, Academic Press, New York, New York, 289.

Montalva, G., N. Bastías, and A. Rodriguez-Marek (2017). Single station sigma in Chile, *16th WCEE*, Santiago, Chile, 9–13 January 2017.

Rodriguez-Marek, A., F. Cotton, N. A. Abrahamson, S. Akkar, L. Al Atik, B. Edwards, G. A. Montalva, and H. M. Dawood (2013). A model for single-station standard deviation using data from various tectonic regions, *Bull. Seismol. Soc. Am.* **103,** 3149–3163.

Rodriguez-Marek, A., G. A. Montalva, F. Cotton, and F. Bonilla (2011). Analysis of single-station standard deviation using the KiK-net data, *Bull. Seismol. Soc. Am.* **101,** 1242–1258.

Seyhan, E., J. P. Stewart, T. D. Ancheta, R. B. Darragh, and R. W. Graves (2014). NGA-West2 site database, *Earthq. Spectra* **30,** 1007–1024.

Wang, C. Y., W. B. Han, J. P. Wu, H. Lou, and W. W. Chan (2007). Crustal structure beneath the eastern margin of the Tibetan plateau and its tectonic implications, *J. Geophys. Res.* **112,** no. B7, doi: 10.1029/2005JB003873.

Wang, H. Y., and S. Y. Wang (2015). A new method for estimating V_{S30} from a shallow shear-wave velocity profile (depth < 30 m), *Bull. Seismol. Soc. Am.* **105,** 1359–1370.

Wang, Y. S., X. J. Li, and Z. H. Zhou (2013). Research on attenuation relationships for horizontal strong ground motions in Sichuan-Yunnnan region, *Acta Seismol. Sinica* **35,** 238–239 (in Chinese).

Wen, R. Z., and Y. F. Ren (2014). Strong-motion observations of the Lushan earthquake on 20 April 2013, *Seismol. Res. Lett.* **85,** 1043–1055.

Wessel, P., and W. H. F. Smith (1991). Free software helps map and display data, *Eos Trans. AGU* **72,** 441.

Yu, T., and X. J. Li (2012). Attenuation relationship of ground motion for Wenchuan earthquake region based on NGA model, *Chinese J. Geotech. Eng.* **34,** 552–558 (in Chinese).

Zafarani, H., and M. R. Soghrat (2017). Single-station sigma for the Iranian strong motion stations, *Pure Appl. Geophys.* **3,** 1–23.

Institute of Engineering Mechanics, China Earthquake Administration
Key Laboratory of Earthquake Engineering and Engineering Vibration of China Earthquake Administration
No. 29 Xuefu Road
Harbin 150080, China
ruizhi@iem.ac.cn
xupeibin13@126.com
whw1990413@163.com
renyefei@iem.net.cn

Manuscript received 22 September 2017;
Published Online 3 July 2018